“© 2015 IEEE. Personal use of this material is permitted. Permission from IEEE must be obtained for all other uses, in any current or future media, including reprinting/republishing this material for advertising or promotional purposes, creating new collective works, for resale or redistribution to servers or lists, or reuse of any copyrighted component of this work in other works.”

A Comparative Study of Coherent Time Reversal Minimum Variance Beamformers for Breast Cancer Detection

Md. Delwar Hossain[1], Ananda Sanagavarapu Mohan[1]
[1] Centre for Health Technologies, University of Technology, Sydney, Australia
Md.D.Hossain@student.uts.edu.au, Ananda.Sanagavarapu@uts.edu.au

***Abstract*— In this study we consider coherent processing for time reversal microwave imaging for breast cancer detection. We derive coherent time reversal standard Capon beamformer (C-TR-SCB) and coherent time reversal robust Capon beamformer (C-TR-RCB) and compare their imaging performances for breast cancer detection in anatomically realistic heterogeneous 3-D breast phantoms.**

***Index Terms*— time reversal, coherent focusing, wavefield modeling, standard Capon beamformer, robust Capon beamformer, breast cancer, microwave imaging.**

I. INTRODUCTION

Microwave radar imaging [1-3] as well as tomography [4-6] have been actively considered for breast cancer detection. Time reversal imaging belongs to a class of radar imaging that is suitable for imaging in cluttered heterogeneous media [7-11]. Breast cancer detection becomes increasingly challenging with increasing breast density as the dielectric property contrast between malignant and healthy, dense glandular tissues is quite low [12, 13].

In time reversal imaging for the detection of breast cancer, ultrawideband pulses are radiated from the antenna elements into the breast and the received backscattering responses are collected at the receiver antenna elements which are usually arranged in a multi-static configuration around the breast. The dense breasts form a highly cluttered medium, which may introduce random phase variations in the backscattering responses from the tumors leading to non-uniform signal subspace over the entire bandwidth. As a result, for conventional frequency domain time reversal imaging, when the received responses are processed incoherently, imaging performance deteriorates due to increasing clutter from tissue heterogeneity.

In this paper, we propose to investigate the advantages of coherent processing for time reversal imaging that incorporates minimum variance beamforming techniques when employed for breast cancer detection in denser breasts. The performance of conventional time reversal standard Capon beamformer (TR-SCB) and the time reversal robust Capon beamformer (TR-RCB) [14] get deteriorated due to the effects of clutter and heterogeneity of the breast medium. To overcome these effects, we propose to derive coherent-TR-SCB (C-TR-SCB) and coherent-TR-RCB (C-TR-RCB) imaging techniques and compare their imaging performance to detect breast cancer in heterogeneous breasts employing MRI derived, anatomically realistic, 3-D numerical breast phantoms [10].Our simulation results indicate that coherent TR-RCB (C-TR-RCB) has superior imaging performance in heterogeneous breast medium.

II. FORMULATION FOR TIME REVERSAL IMAGING

Let us consider a cylindrical antenna array consisting of N antenna elements in a 3-D bounded region. We assume that there are P targets embedded in the background medium with known dielectric properties. The targets are assumed to be small spherical isotropic dielectric spheres. The dielectric tensor of the p-th target is given as $\varepsilon_p^x = \varepsilon_p^y = \varepsilon_p^z = \varepsilon_p$. The multistatic matrix thus can be expressed as

$$\overline{\mathbf{K}} = \overline{\boldsymbol{\mathcal{G}}}\,\overline{\boldsymbol{\chi}}\,\overline{\boldsymbol{\mathcal{G}}}^{T} + \sigma^2 \overline{\mathbf{I}} \tag{1}$$

where, $\overline{\boldsymbol{\chi}}$ is $3P\times 3P$ a matrix representing the polarization tensors of the P targets, $\overline{\boldsymbol{\mathcal{G}}}$ is a $3N\times 3P$ matrix obtained from the background medium green's function and σ^2 is the noise variance of the additive white Gaussian noise (AWGN).

The time reversal operator (TRO) can be interpreted as the covariance matrix [15] and defined in frequency domain as

$$\overline{\mathbf{T}}(\omega) = \overline{\mathbf{K}}^{H}(\omega)\overline{\mathbf{K}}(\omega) \tag{2}$$

In frequency domain, conventional, time reversal imaging, the whole ultrawideband is divided into a number of narrow frequency bins and imaging is performed using the TRO at each frequency bin which are then combined to obtain the ultrawideband time reversal image. As increased tissue clutter and heterogeneity produces random phase variation, the signal subspace of TRO becomes non-uniform over the ultrawideband frequency range.

III. COHERENT FOCUSING FOR TRO

In coherent time reversal imaging approach, the individual TROs at each frequency bin are coherently focused to result in a coherently focused TRO (C-TRO). When time reversal imaging is carried using C-TRO, the coherently focused

energy results in stronger focusing intensity at the target location compared to non-coherent time reversal imaging. Coherent time reversal minimum variance beamforming was first proposed in [14] for 2-D acoustic imaging which employed the focusing matrix derived using the coherent signal subspace method. Here, we propose a different approach to derive the coherent focusing matrix using wavefield modeling method [16]. Considering the locations of P embedded targets to be uniformly distributed independent discrete random variables, we compute the focusing matrix, $\bar{\mathbf{Z}}^H$ by minimizing the focusing error given by

$$\min_{\bar{\mathbf{Z}}(\omega_f)} E_{\mathbf{r}^o}\left\{\left\|\bar{\boldsymbol{\mathcal{G}}}(\omega_0)-\bar{\mathbf{Z}}^H(\omega_f)\bar{\boldsymbol{\mathcal{G}}}(\omega_f)\right\|^2\right\} \tag{3}$$

where, $E_{\mathbf{r}^o}\{.\}$ is the expectation operator and $\|.\|$ denotes the Frobenius norm. The focusing matrix is computed by minimizing the focusing error given as [16]

$$\tilde{e}^2=\frac{1}{N}\int_V d\mathbf{r}\left\|e_{\mathbf{r}}(\omega_f)\right\|^2=\frac{1}{N}\left\|\bar{\mathbf{F}}(\omega_0)-\bar{\mathbf{Z}}^H(\omega_f)\bar{\mathbf{F}}(\omega_f)\right\|^2 \tag{4}$$

where, $\bar{\mathbf{F}}$ is the array sampling matrix obtained using the spherical harmonic expansion [17]. Hence, the C-TRO can be obtained as

$$\bar{\mathbf{T}}_C(\omega_o)=\sum_{f=1}^{F}\bar{\mathbf{Z}}(\omega_f)\bar{\mathbf{T}}(\omega_f)\bar{\mathbf{Z}}^H(\omega_f) \tag{5}$$

Now we can use C-TRO in (5) over a limited number of focused frequency bins for imaging rather than using all the frequency bins.

A. Coherent Time Reversal Standard Capon Beamformer

The incoherent TRO at each frequency bin when coupled with the covariance matrix of the standard Capon beamformer (SCB) results in TR-SCB. Instead of using incoherent TRO at each frequency bin, we propose to employ the C-TRO with SCB to obtain coherent TR-SCB (C-TR-SCB). The array weight vector, $\bar{\mathbf{w}}$ for C-TR-SCB can then be estimated as

$$\min_{\bar{\mathbf{w}}}\bar{\mathbf{w}}^H\bar{\mathbf{T}}_C\bar{\mathbf{w}}\quad\text{subject to}\quad\bar{\mathbf{w}}^H\bar{\mathbf{g}}(\mathbf{r})=1 \tag{6}$$

where, $\bar{\mathbf{g}}$ is the Green's function vector of the background medium. The imaging function for C-TR-SCB is given by

$$I_{C-TR-SCB}(\mathbf{r})=\left\|\bar{\tilde{\mathbf{w}}}^H(\mathbf{r})\bar{\mathbf{T}}_C^{-1}\bar{\tilde{\mathbf{w}}}(\mathbf{r})\right\|^2 \tag{7}$$

B. Coherent Time Reversal Robust Capon Beamformer

The RCB modifies SCB to minimize the sensitivity to array steering vector mismatch [14]. The robustness is achieved by considering the uncertainty about steering vector. For time reversal imaging, the TR-RCB can be superior to TR-SCB as it is less sensitive to green's function vector mismatch. We derive robust estimator for σ^2 from the C-TRO as

$$\max_{\sigma^2,\bar{\mathbf{g}}}\ \sigma^2\quad\textit{subject to}\quad\bar{\mathbf{T}}_C-\sigma^2\bar{\bar{\mathbf{g}}}\bar{\bar{\mathbf{g}}}^H\geq 0,\qquad\left\|\bar{\mathbf{g}}-\bar{\tilde{\mathbf{g}}}\right\|^2\leq\varphi \tag{8}$$

This optimization problem can be reduced to

$$\min_{\bar{\mathbf{g}}}\ \bar{\mathbf{g}}^H\bar{\mathbf{T}}_C^{-1}\bar{\mathbf{g}}\quad\text{subject to}\quad\left\|\bar{\mathbf{g}}-\bar{\tilde{\mathbf{g}}}\right\|^2=\varphi \tag{9}$$

Using the Lagrange multiplier methodology [14], the weight vector, $\bar{\tilde{\mathbf{w}}}$ can be estimated for C-TR-RCB imaging. Consequently, the imaging function for the C-TR-RCB is obtained as

$$I_{C-TR-RCB}(\mathbf{r})=\left\|\bar{\tilde{\mathbf{w}}}^H(\mathbf{r})\bar{\mathbf{T}}_C\bar{\tilde{\mathbf{w}}}(\mathbf{r})\right\|^2 \tag{10}$$

IV. FDTD Simulation using Numerical Breast Phantoms

We employ FDTD simulation using anatomically realistic numerical breast phantoms obtained from UWCEM breast phantom repository [9]. We use a cylindrical antenna array consisting of 5×23 UWB antenna elements to record the scattered field response from the breast. We consider ideal antenna elements for simulation. We use a differentiated Gaussian pulse excitation with a 3dB bandwidth 1-5GHz. The FDTD grid size is set to 0.5mm in all directions and computational domain is truncated using perfectly matched layer (PML) boundary. It is assumed that the patient is lying in supine position and the breast is inserted into the cylindrical array. We consider single pole Debye parameters [12, 13] to model the dispersive dielectric properties of different breast tissues. The dielectric map of a heterogeneously dense (C3) breast phantom at 3GHz along with the simulation set-up is illustrated in Fig. 1. A 10mm sized malignant tissue (tumor) is inserted into a pre-determined location in the breast to mimic a patient with breast cancer. In order to reduce mismatches from the breast skin, the breast phantom and the antenna array are assumed to be immersed into a coupling liquid. A C3 breast may contain upto 75% glandular tissue content while a breast with scattered heterogeneity (C2) is composed of upto 50% glandular tissues. We consider both C2 and C3 breast phantoms for simulations. Once the scattered fields are obtained, we remove the skin reflection from early time response as described in [11]. The artifact free scattered response is then used for time reversal imaging.

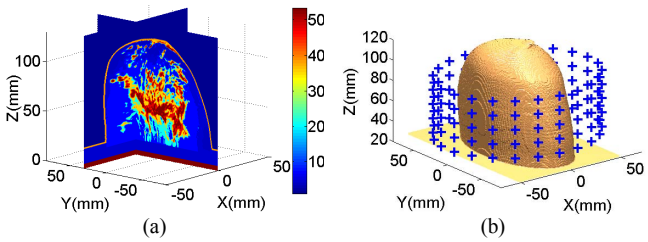

Fig. 1. A heterogeneously dense (C3) breast phantom (a) dielectric map, (b) simulation set-up.

V. RESULTS

Firstly, we compare the results obtained from conventional and coherently processed TR-SCB, TR-RCB for a C2 breast phantom as shown in Figs. 2-3. It can be observed that the TR-SCB image has peak intensity near the actual tumor location indicated using the spherical inclusion. However, there are strong side lobes outside the region of focus. The coherent version, viz., C-TR-SCB obtains an improved imaging performance compared with TR-SCB, as the side lobes are significantly reduced.

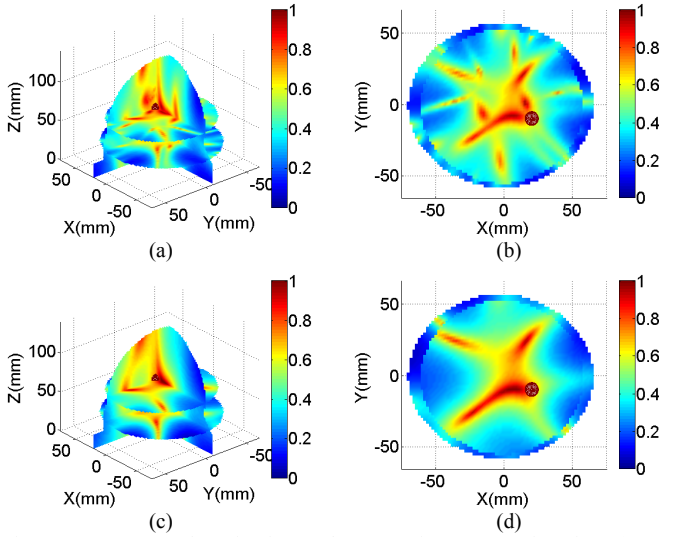

Fig. 2. Breast cancer detection in C2 phantom using TR-SCB imaging (a) 3-D view, (b) coronal cut, C-TR-SCB imaging (c) 3-D view, (d) coronal cut.

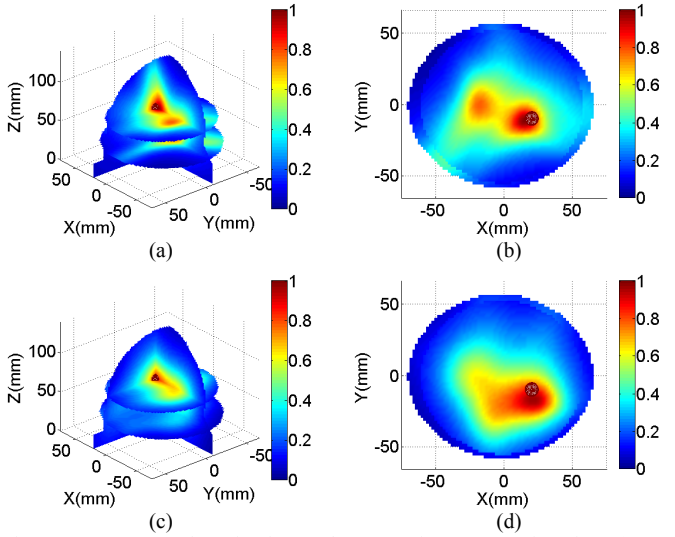

Fig. 3. Breast cancer detection in C2 phantom using TR-SCB imaging (a) 3-D view, (b) coronal cut, C-TR-SCB imaging (c) 3-D view, (d) coronal cut.

It can also be observed that the TR-SCB cannot accurately estimate the tumor location as there are multiple high intensity peaks away from the actual tumor location. On the other hand, the C-TR-SCB provides improved imaging results as side lobes decrease considerably and peak image intensity is focused closer to the true tumor location compared to that of TR-SCB. Now consider the TR-RCB. As shown in Fig. 3, it obtains superior imaging performance as the side lobes are considerably weaker and tumor location can be quite accurately estimated. The C-TR-RCB further improves the performance as it reduces the effects of clutter which is evident from waning side lobes.

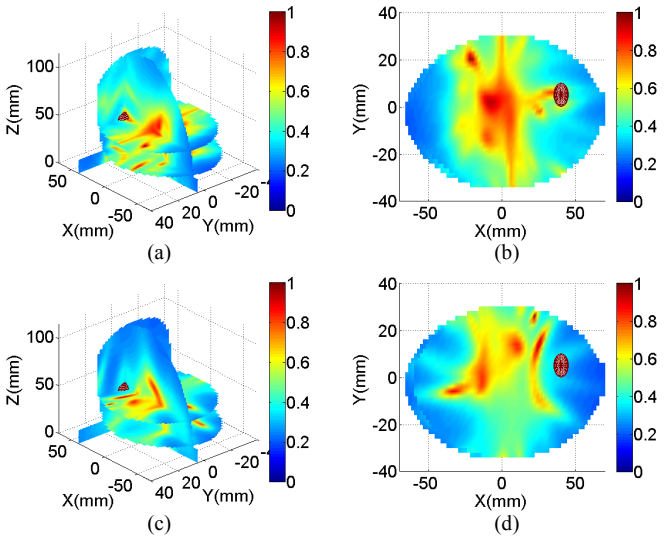

Fig. 4. Breast cancer detection in C3 phantom using TR-SCB imaging (a) 3-D view, (b) coronal cut, C-TR-SCB imaging (c) 3-D view, (d) coronal cut.

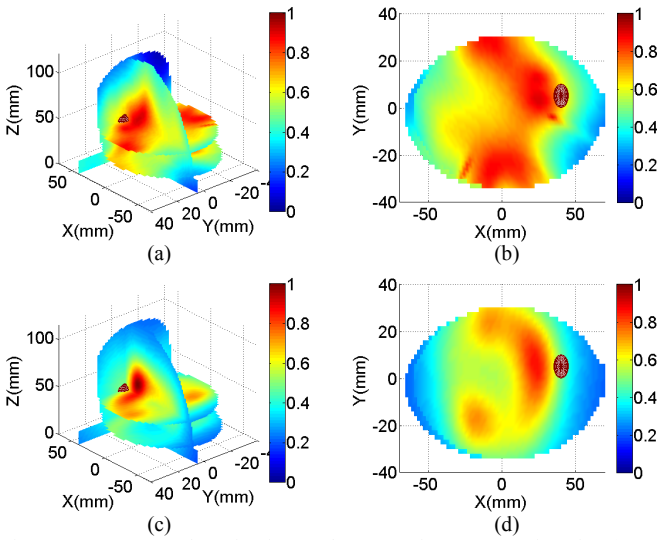

Fig. 5. Breast cancer detection in C3 phantom using TR-RCB imaging (a)3-D view, (b) coronal cut, C-TR-RCB imaging (c) 3-D view, (d) coronal cut.

Now let us consider the imaging results for the C3 breast phantom. A C3 breast contains higher amounts of dense glandular tissues than C2 breast and hence poses higher challenges for microwave imaging. As shown in Fig. 4, the TR-SCB image has peak intensity away from the actual tumor location and shows multiple high intensity peaks as well. This is due to the scattering from of higher amounts of dense glandular tissues in the C3 breast. The proposed C-TR-SCB

shows improved imaging performance compared to TR-SCB although there are some strong side lobes present. For C-TR-SCB, most importantly the peak intensity region is closer to the actual tumor location in the image.

TR-RCB and C-TR-RCB imaging results for the C3 breast phantom are shown in Fig. 5. It can be observed from Fig. 5(a)-(b) that TR-RCB provides superior imaging performance compared to TR-SCB in spite of significantly high side lobes arising from highly cluttered C3 breast tissue medium. However, C-TR-RCB provides satisfactory imaging results as the highest intensity of the image is in the close vicinity of the actual tumor location. Remarkably C-TR-RCB image shows the least amounts of side lobes among the techniques compared here. The images in Figs. 2-5 have been obtained at SNR=40dB.

VI. Conclusion

The imaging results demonstrate the requirement for coherent focusing for time reversal imaging for breast cancer detection. It is clearly observed that non-coherent TR-SCB and TR-RCB performs poorly compared to coherent techniques C-TR-SCB and C-TR-RCB in both C3 and breast phantoms. However, the coherent imaging performance is considerably superior for C3 breast phantom compared to C2 breast phantom. This is because of the presence of higher amounts of dense glandular tissues in the C3 breast. Hence, coherent imaging can be useful when the breast tissue heterogeneity is higher. It is also found that the performance of TR-RCB and its coherent counterpart is superior as they are less sensitive to mismatch of Green's functions. Although the actual breast tissue medium is heterogeneous, an equivalent, virtual homogeneous medium is employed for using synthetic time reversal imaging. In general, the actual breast tissue heterogeneity is unknown and it is also quite challenging to derive the Green's function of the breast medium even if the breast heterogeneity is known. This mismatch in Green's functions result in a small bias in tumor location estimation for both TR-RCB and C-TR-RCB imaging techniques. However, the C-TR-RCB obtains tumor location with a reasonable accuracy and greatly eliminates high side lobes resulting from glandular tissue scattering. We can conclude that coherent processing can help to reduce the detrimental effects arising from strong clutter in the imaging medium. Coherent processing also reduces the computational burden as imaging is carried out only for the coherently focused bin instead of imaging at each frequency bin.

Acknowledgment

This work was supported by the Australian Research Council under Discovery Grant DP 0773234.

References

[1] H. F. Abutarboush and M. Klemm, "Signal Selection for Contrast-Enhanced UWB Microwave Radar Imaging With Inhomogeneous Breast Phantoms," *IEEE Antennas Wireless Propag. Lett.,* vol. 12, pp. 1408-1411, 2013.

[2] E. C. Fear, J. Bourqui, C. Curtis, D. Mew, B. Docktor, and C. Romano, "Microwave Breast Imaging With a Monostatic Radar-Based System: A Study of Application to Patients," *IEEE Trans. Microw. Theory Tech.,* vol. 61, pp. 2119-2128, 2013.

[3] E. Porter, E. Kirshin, A. Santorelli, M. Coates, and M. Popovic, "Time-Domain Multistatic Radar System for Microwave Breast Screening," *IEEE Antennas Wieless Propag. Lett.,* vol. 12, pp. 229-232, 2013.

[4] P. K. J. D. Shea, S. C. Hagness, B. D. Van Veen, "Contrast-enhanced microwave imaging of breast tumors: A computational study using 3D realistic numerical phantoms," *Inverse Problems,* vol. 26, p. 22, 2010.

[5] P. M. Meaney, A. H. Golnabi, N. R. Epstein, S. D. Geimer, M. W. Fanning, J. B. Weaver, and K. D. Paulsen, "Integration of microwave tomography with magnetic resonance for improved breast imaging," *Med. Phy.,* vol. 40, p. 103101(pp13), 2013.

[6] A. E. Fouda and F. L. Teixeira, "Ultra-wideband microwave imaging of breast cancer tumors via Bayesian inverse scattering," *J. Appl. Phys.,* vol. 115, p. 064701(pp8), 2014.

[7] P. Kosmas and C. M. Rappaport, "A matched-filter FDTD-based time reversal approach for microwave breast cancer detection," *IEEE Trans. Antennas Propag.,* vol. 54, pp. 1257-1264, 2006.

[8] P. Kosmas and C. M. Rappaport, "FDTD-based time reversal for microwave breast cancer Detection-localization in three dimensions," *IEEE Trans. Microw. Theory Tech.,* vol. 54, pp. 1921-1927, 2006.

[9] Y. Chen, E. Gunawan, L. Kay Soon, W. Shih-chang, K. Yongmin, and S. Cheong-Boon, "Pulse Design for Time Reversal Method as Applied to Ultrawideband Microwave Breast Cancer Detection: A Two-Dimensional Analysis," *IEEE Trans. Antennas Propag.,* vol. 55, pp. 194-204, 2007.

[10] Y. Chen, E. Gunawan, L. Kay Soon, W. Shih-chang, S. Cheong-Boon, and T. C. Putti, "Time-Reversal Ultrawideband Breast Imaging: Pulse Design Criteria Considering Multiple Tumors With Unknown Tissue Properties," *IEEE Trans. Antennas Propag.,* vol. 56, pp. 3073-3077, 2008.

[11] M. D. Hossain, A. S. Mohan, and M. J. Abedin, "Beamspace Time-Reversal Microwave Imaging for Breast Cancer Detection," *IEEE Antennas Wieless Propag. Lett.,* vol. 12, pp. 241-244, 2013.

[12] M. Lazebnik, M. Okoniewski, J. H. Booske, and S. C. Hagness, "Highly accurate debye models for normal and malignant breast tissue dielectric properties at microwave frequencies," *IEEE Microw. Wireless Comp. Lett.,* vol. 17, pp. 822-824, 2007.

[13] M. Lazebnik, et al., "A large-scale study of the ultrawideband microwave dielectric properties of normal, benign and malignant breast tissues obtained from cancer surgeries " *Phy. Med. Biol.,* vol. 52, pp. 6093–6115, 2007.

[14] Z. Wang, J. Li, and R. Wu, "Time-delay- and time-reversal-based robust capon beamformers for ultrasound imaging," *IEEE Trans. Med. Imag.,* vol. 24, pp. 1308-1322, 2005.

[15] P. Claire and J. Thomas, "Experimental subwavelength localization of scatterers by decomposition of the time reversal operator interpreted as a covariance matrix," *J. Acoust. Soc. Am.,* vol. 114, pp. 235-243, 2003.

[16] Y. Bucris, I. Cohen, and M. A. Doron, "Bayesian Focusing for Coherent Wideband Beamforming," *IEEE Trans. Audio, Speech, Language Process.,* vol. 20, pp. 1282-1296, 2012.

[17] M. A. Doron and E. Doron, "Wavefield modeling and array processing - I. Spatial sampling," *IEEE Trans. Signal Process.,* vol. 42, pp. 2549-2559, 1994.